

We are IntechOpen, the world's leading publisher of Open Access books Built by scientists, for scientists

4,800

Open access books available

122,000

International authors and editors

135M

Downloads

Our authors are among the

154

Countries delivered to

TOP 1%

most cited scientists

12.2%

Contributors from top 500 universities



WEB OF SCIENCE™

Selection of our books indexed in the Book Citation Index
in Web of Science™ Core Collection (BKCI)

Interested in publishing with us?
Contact book.department@intechopen.com

Numbers displayed above are based on latest data collected.
For more information visit www.intechopen.com



Electromagnetic Field Interaction with Metamaterials

Mohammed M. Bait-Suwailam

Abstract

It is well known that constitutive parameters, namely, the electrical permittivity, ϵ , and the magnetic permeability, μ , in a medium determine the response and reaction of such medium or material when exposed to external time-varying electromagnetic fields. Furthermore, most materials are lossy and dispersive, that is, both permittivity and permeability are complex and frequency-dependent. Interestingly, by controlling the sign of real parts of ϵ and μ in a medium, unique electromagnetic properties can be achieved that are not readily available in nature. Recently, subwavelength composite engineered structures, also known as *metamaterials*, have evolved in many engineering and optical applications, due to their unique electromagnetic properties that are not found in nature, including but not limited to negative refractive index, backward wave propagation, subwavelength focusing and super lenses, and invisibility cloaking. The main aims of this chapter are to provide an overview of electromagnetic field behavior and interaction with metamaterials and to explore such behavior in various metamaterials both analytically and numerically.

Keywords: double negative medium, electromagnetic waves, metamaterials, plane wave, single-negative medium

1. Introduction

Electromagnetic field is a physical behavior that is produced in a space due to time-varying electric charges and represents the interaction between electric and magnetic fields. Unlike static charges that can only produce static electric fields in space, time-varying electric charges are one of sources for the rise of magnetic fields, which in turn produce time-varying electric fields. This is summarized in the four time-varying Maxwell's equations given in differential form:

$$\nabla \cdot \mathbf{E} = \rho_v(t)/\epsilon \quad (1)$$

$$\nabla \cdot \mathbf{B} = 0 \quad (2)$$

$$\nabla \times \mathbf{E} = -\mu \frac{\partial \mathbf{H}}{\partial t} \quad (3)$$

$$\nabla \times \mathbf{B} = \mathbf{J}(t) + \epsilon \frac{\partial \mathbf{E}}{\partial t} \quad (4)$$

where ρ_v is time-varying volume charge density, ϵ and μ are the electric permittivity and magnetic permeability, respectively, \mathbf{J} is the time-varying electric current

density in a medium, \mathbf{D} and \mathbf{B} are time-varying electric and magnetic flux densities, respectively, and \mathbf{E} and \mathbf{H} are time-varying electric and magnetic field intensities, respectively.

In 1864, James Maxwell showed through Eqs. (1)–(4) that oscillating electric and magnetic fields give rise to electromagnetic waves that travel at the speed of light in free space [1], which also implies that light is electromagnetic in nature. By taking the curl of Eqs. (3) and (4), it is also straightforward to show that electromagnetic wave propagation can exist.

In a medium, there are two main quantities, also known as the constitutive parameters, namely, electric permittivity, ϵ , and the magnetic permeability, μ , in addition to the conductivity, σ , that determine the nature of electromagnetic wave and its behavior in such a medium. In other words, the aforementioned parameters along with the boundary conditions in a medium determine uniquely the response of such medium to an incoming electromagnetic wave. This is also summarized through two equations, given below, that describe the relationship between electric and magnetic field quantities in a simple linear and isotropic medium:

$$\mathbf{D} = \epsilon \mathbf{E} \quad (5)$$

$$\mathbf{B} = \mu \mathbf{H} \quad (6)$$

where in Eqs. (5)–(6), both ϵ and μ in a lossy dispersive medium are commonly complex and frequency-dependent and are real quantities in a lossless isotropic medium. From such relations, Eqs. (1)–(6), important parameters, such as the wavenumber, k , the refractive index, n , and the intrinsic wave impedance, η , in a medium can be determined, which are given respectively as:

$$k = \omega \sqrt{\mu \epsilon} \quad (7)$$

$$\eta = \sqrt{\mu / \epsilon} \quad (8)$$

$$n = \sqrt{\mu_r \epsilon_r} \quad (9)$$

where $\omega = 2\pi f$ is the radian frequency (in rad/sec), f is the frequency (in Hz), and $\mu_r = \mu/\mu_0$ and $\epsilon_r = \epsilon/\epsilon_0$ are the relative permeability and permittivity, respectively, while μ_0 and ϵ_0 are the free-space permeability and permittivity, respectively.

2. Overview of metamaterials and their realizations

Figure 1 depicts a general overview of possible materials based on their constitutive parameters: the electric permittivity and the magnetic permeability values. The aforementioned constitutive parameters are in principle complex, and their signs are based on the signs of their real parts, while their imaginary parts indicate the presence of electric or magnetic losses, respectively. While in naturally occurring materials, both real parts of the permittivity and permeability are positive (i.e., >0); it is possible that either one of the real parts of the constitutive parameters or even both have negative values. In the second quadrant, while permeability is above zero, the permittivity is below zero (negative), which can be termed as a single-negative (SNG) or ϵ -negative (ENG) medium. Similarly, when a medium possesses negative permeability value, while its permittivity is positive, this is also termed as an SNG medium or μ -NG (MNG) medium, where $\mu < 0$ in this type of material, as shown in the third quadrant in **Figure 1**. An interesting medium is the case when both real parts of permittivity and permeability are negative (i.e., the third quadrant in **Figure 1**). This is termed as double negative (DNG) medium or left-handed

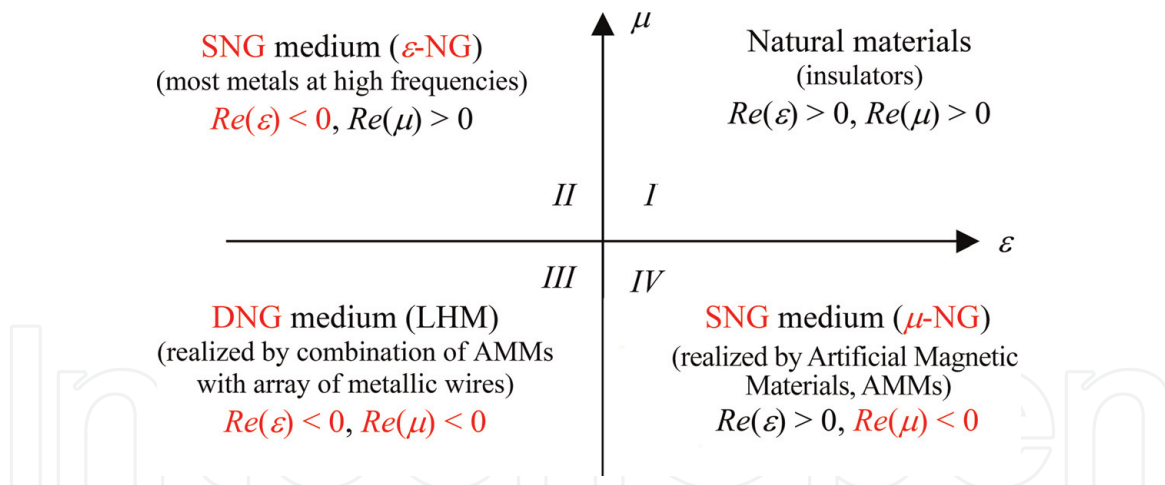


Figure 1.
 Classification of materials, based on their constitutive parameters, ϵ and μ .

medium (LHM), due to its unique resultant electromagnetic features, like negative refraction and negative phase velocity, as it follows a left-handed system rule. In summary, metamaterials have three classes, depending on the signs of their constitutive parameters: ENG, MNG, and DNG.

Practically, natural SNG media are available that possess ENG response, for instance, metals at visible and near-ultraviolet regime. However, at much lower frequencies, one commonly adopted realization of SNG medium is the periodic arrangement of metallic wires, which results in possessing negative effective permittivity below the plasma frequency of metallic wires or rods [2]. It is instructive to mention here that naturally occurring materials with permeability values below zero are not yet available in nature, especially within the radio frequency/microwave regime. However, such response can be obtained through engineered arrangement of metallic inclusions printed on a dielectric medium [3], as it will be discussed further later on.

After the seminal work of Veselago in [4], where he investigated mathematically the possibility of electromagnetic wave propagation through materials with both negative permittivity and permeability values, the word “metamaterials” evolved, which refers to what is beyond naturally occurring materials. Metamaterials can be defined as artificially engineered structures that have electromagnetic properties not yet readily available in nature. Such artificial composite structures are realized in one way by periodically patterning metallic resonant inclusions in a host medium, i.e., dielectric or magneto-dielectric material, either in a symmetric or nonsymmetric fashion. When exposed to an electromagnetic field, the metamaterials alter the electromagnetic properties of the new host medium due to mainly the inclusions’ response and features. **Figure 2** depicts a general view of one possible realization of a metamaterial structure.

Tremendous efforts had been put forward in the past with the goal to provide efficient numerical means for the retrieval of constitutive parameters of arrays of metamaterials in order to advance the design and characterization of metamaterials [5–7]. Such numerical retrievals provided engineering and physical means in replacing local electromagnetic response details of individual metamaterials elements with averaged or homogenized values for the effective electric permittivity, ϵ_{eff} , and effective magnetic permeability, μ_{eff} . As a matter of fact, this retrieval approach is a direct translation of the characterization of natural media, which consist of atoms and molecules with their dimensions that are much smaller in magnitude than the wavelength. The electromagnetic wave response and propagation within the effective metamaterial medium can then be fundamentally

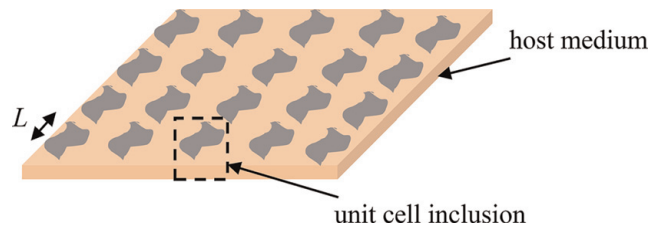


Figure 2.
General sketch of a metamaterial composite structure.

described using constitutive parameters along with Maxwell's equations. In principle, this effective response would be permissible if the unit cell dimension is sufficiently small enough or a fraction of an operating wavelength [5], say, for example, L , as shown in **Figure 2**, satisfies the relation below:

$$L \ll \lambda \quad (10)$$

where L is the unit cell dimension and λ is the operating wavelength of the incoming electromagnetic field. When the condition in Eq. (10) holds, quasi-static behavior for the artificial metamaterials can be applied, in which an equivalent resonant circuit, composed of *resistor-inductor-capacitor (RLC) elements*, is permissible to use in order to provide qualitative description of the physical behavior of the artificial materials [8].

2.1 Realization of artificial μ -negative (MNG) medium

Among engineered materials with negative magnetic permeability, artificial magnetic materials (AMMs) have been the subject of interest for many years. This is due to their unique features, including low cost ease of integration with radio frequency/microwave circuits, and the possibility of synthesizing magnetic permeability to certain magnetization and polarization levels at the frequency of interest. This is in contrast to ordinary magnetic materials, like ferrite composites, that are limited in their magnetization levels and as well as suffer from magnetic losses at microwave frequency regime [9].

The idea of creating magnetic materials from conductors was first proposed by Schelkunoff [10]. A wide variety of artificial magnetic inclusions have been proposed and implemented in the literature. One of the popular and widely applied artificial magnetic materials is the split-ring resonator (SRR). Pendry et al. [3] used concentric metallic rings in order to provide further enhancement of the magnetic properties of the rings. The SRR, as shown in **Figure 3a**, consists of two concentric circular (i.e., edge-coupled) metallic rings printed in a host dielectric medium, with splits at opposite ends of the rings. Another form of "SRR-based" AMM is realized by placing the two split-rings in opposite sides (broadside-coupled) within the host medium [11, 12], which can provide two advantages: firstly, the effects of bianisotropy, or cross polarization, are eliminated due to the broadside nature of the metallic rings (see **Figure 3c**), and secondly, there is additional capacitive coupling to the composite structure, hence achieving stronger resonance behavior [8, 11, 12], as shown in **Figure 3b**. Other forms of resonant metallic inclusions, like spiral, omega, Hilbert, can also be adopted to achieve artificial magnetic media, as shown in **Figure 3**. Significant miniaturization factors can be achieved using either spiral- or Hilbert-type resonators [13, 14].

The physical principle of operation behind the artificial magnetic materials, as shown in **Figure 3**, is almost the same. Let us consider the subwavelength resonant inclusion in **Figure 3c** and assume that it occupies an infinite space with large number

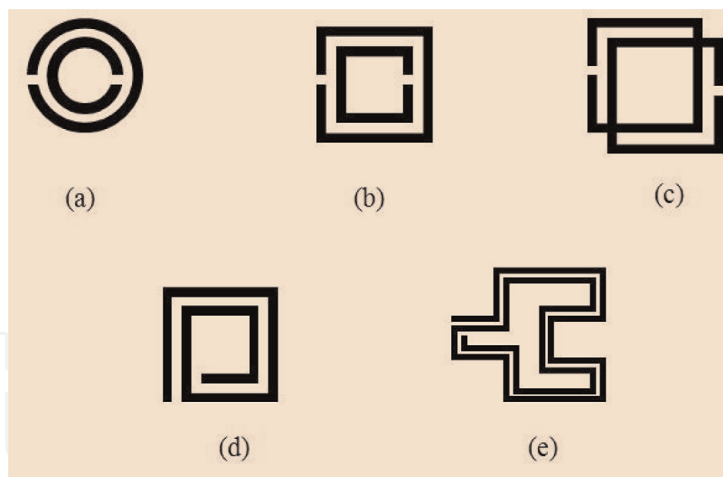


Figure 3. Possible resonant metallic inclusions for synthesizing artificial magnetic materials, (a) edge-coupled circular SRR, (b) edge-coupled square SRR, (c) broadside-coupled SRR, (d) spiral resonator, and (e) Hilbert resonator.

of periodicity in two- or three-dimensional planes (i.e., periodicity implies here repetition factor that is much smaller than λ). Upon an excitation of an external magnetic field, which is orthogonal to the paper plane, to such an infinitely large and homogenized artificial structure, the external magnetic field induces an electromotive force in the inclusions, which in turn results in a circulating effective current flowing around the inclusions. Upon such excitation, a general form for the effective magnetic permeability of any of the AMM structures as shown in **Figure 3** can then be expressed as

$$\mu_{eff} = 1 - \frac{K j\omega L_{eff}}{Z_{inc} + j\omega L_{eff}} \quad (11)$$

where K is a normalized fractional surface area that is enclosed by the AMM inclusion and L_{eff} is the effective inductance of the AMM, which is given by

$$L_{eff} = \frac{\mu_0 S}{p} \quad (12)$$

where S is the surface area of the AMM and p is the periodicity of the AMM inclusion that mimics an infinitely large AMM structure. The parameter Z_{inc} in Eq. (11) consists of two parts: R_{eff} , which represents the encountered ohmic losses due to the finite conductivity of the metallic rings within the AMM inclusions, and C_{eff} , which is the mutual capacitive effect due to the close proximity of the AMM metallic rings/strips. Comprehensive analytical modeling approaches can be found in [3, 8, 12–14].

2.2 Realization of artificial ϵ -negative (ENG) medium

As discussed in the previous section, the realization of metallic resonant inclusions patterned in a homogenized host medium had made it possible to synthesize magnetic permeability in the microwave and optical regimes [3]. Similarly, it is possible to engineer the permittivity of a bulk medium by facilitating patterned metallic inclusions. In solid metals, negative permittivity response commonly occurs at the visible and near-ultraviolet regime, due to the entire oscillation of plasmons [15]. Pendry et al. showed that an array of thin rods or wires arranged in a cubical lattice can indeed exhibit negative effective permittivity response at the microwave regime given by the Drude function [2]:

$$\varepsilon(\omega) = 1 - \frac{\omega_p^2}{\omega(\omega + j\Gamma)} \quad (13)$$

where Γ is the energy dissipation factor of the plasmon into the system (i.e., damping factor). In solid metals, like aluminum, the dissipation factor, Γ , is usually small as compared to the plasmon frequency, ω_p . If losses were neglected, (i.e., $\Gamma \approx 0$), it is evident from Eq. (13) that electromagnetic waves below the plasma frequency ($\omega < \omega_p$) cannot propagate, since $\varepsilon < 0$ (μ here > 0). It is also evident from Eq. (13) that the refractive index, n , will be imaginary and a wave in such a medium will be evanescent.

The electric permittivity response in Eq. (13) can be used to represent the effective electrical permittivity response of a synthesized homogeneous medium comprising an array of very thin metallic wires. Note that in the realization of the composite periodic lattice of wires, wires' diameter is essentially much smaller than the operating wavelength in order to mimic an effective homogenized negative permittivity media from such periodic metal rods. The term ω_p represents the plasma frequency for metals and can be expressed in terms of the electron properties by following relation [2]:

$$\omega_p^2 = \frac{nq^2}{\varepsilon_0 m_e} \quad (14)$$

where q is the electron charge, ε_0 is the free-space permittivity, and n and m_e are the effective density and mass of electrons, respectively.

From classical electromagnetic theory, metallic wires behave collectively as small resonant dipoles when excited with an applied electric field parallel to the wires plane, similar to the electric dipoles response of atomic and molecular systems in natural materials [2]. Although the metallic wire structure, discussed earlier, can tailor effective permittivity response within the radio frequency and microwave regime, the arrangement of metallic wires in a cubic structure is still bulky and may appear undesirable for planar radio frequency and microwave applications.

Recently, Falcone et al. introduced in [16–18] a subwavelength resonant planar particle, known as the complementary split-ring resonator (CSRR) as shown in **Figure 4b**, which is the dual counterpart of the SRR. In other words, by following Babinet's principle [19], the complementary of the planar SRR structure is obtained by replacing the SRR metallic rings with apertures and the apertures (surrounding free-space region of SRR) with metal plates. By etching the SRR rings from the metallic ground screen, complementary SRRs form the basis of realizing compact microstrip-based bandstop filters [16]. Such bandstop behavior is attributed to the existence of negative electrical permittivity response, due to an axial time-varying electric field parallel to the CSRR ring plane. Interestingly, as it is practically straightforward to excite CSRR particle with an axial electric field, CSRR particle is very easy to integrate with other planar microstrip circuits.

With the assumption that the largest dimension in CSRR unit cell is much smaller than the operating wavelength, a quasi-static equivalent circuit model can be considered to estimate the effective permittivity response of such inclusion [18].

Consider an axial external uniform time-varying electric field that is parallel to the CSRR inclusion plane, as shown in **Figure 4b**; the composite structure will react and oppose the applied external electric field by creating internal electric dipole moments that give rise to electrical polarization effect. Following the analytical formulation given in [20] and assuming a homogenized artificial CSRR structure, the overall effective electrical permittivity response of the homogenized artificial CSRR structure can then be written in the form below in terms of basic *RLC* circuit elements:

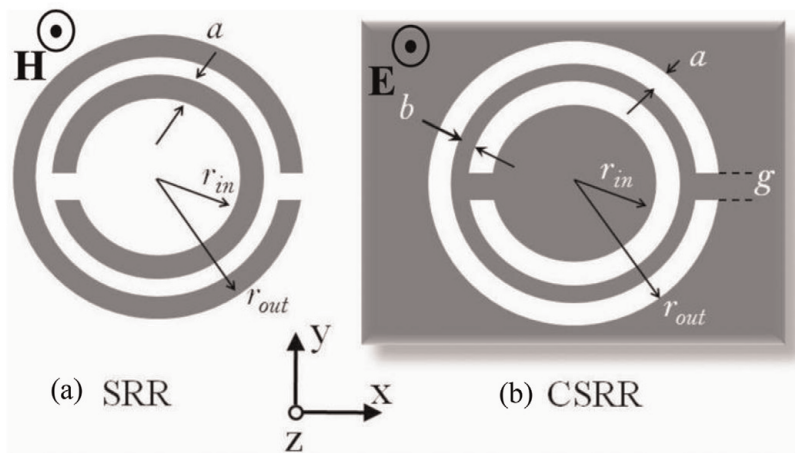


Figure 4. Two-dimensional view of (a) an artificial magnetic material inclusion, the circular SRR; (b) complementary SRR (CSRR), with dimensions; r_{out} is radius of outer ring, r_{in} is internal ring radius, a represents metallic (aperture) width, b is spacing between rings in SRR (spacing between etched rings in CSRR), and g represents the SRR ring's cut (CSRR etched rings' left metallization). The gray area represents structure metallization.

$$\epsilon_{eff} = 1 + \frac{K Z_{inc}}{Z_{inc} + \frac{1}{j\omega C_{eff}}} \quad (15)$$

where K is a normalized fractional surface area of CSRR inclusion and C_{eff} is the effective capacitance of a parallel plate capacitor with surface area being the CSRR inclusion surface, while the thickness of the capacitor is the periodicity of the CSRR as a composite infinitely large structure. The term Z_{inc} in Eq. (15) represents the effective impedance of the CSRR inclusion and is given by

$$Z_{inc} = R_{eff} + j\omega L_{eff} \quad (16)$$

where R_{eff} is the effective ohmic losses due to the finite conductivity of the metallic rings around the CSRR slots and is given by the alternating current resistance of the rings. The term L_{eff} in Eq. (16) accounts for the mutual inductive effects between the external and internal strips around the slotted rings. More analytical modeling of the effective electric permittivity and CSRR equivalent circuit parameters can be found in [18, 20]. **Table 1** summarizes the most common artificial magnetic and electric inclusions (i.e., SRR and its dual, CSRR) in order to realize single- μ NG and $-\epsilon$ NG media, respectively, and their equivalent basic circuit representations (**Figures 5–7**).

2.3 Realization of artificial double negative (DNG) medium

In 1968, Veselago investigated theoretically that electromagnetic waves can propagate in a medium, where both permittivity and permeability are negative [4], which was then termed as metamaterials, DNG media, or LHM materials. The realization of artificial DNG media evolved after the theoretical studies by Pendry in [2, 3] in order to synthesize AMMs and artificial ENG media at low frequencies, and afterward practical realizations and demonstrations of DNG media by Smith and his team in [21, 22], which was achieved by producing a large bulk structure composed of repeated patterns of artificial MNG, in the form of SRRs, and ENG media, in the form of planar metallic strips.

Several interesting properties that are not yet in nature can be achieved with DNG media, including but not limited to backward wave propagation and negatively refracted waves and perfect lens [23].

2.4 Potential applications of metamaterials

Table 2 summarizes possible families of artificial metamaterials based on the signs of their permittivity and permeability, assuming such materials are passive, along with a list of suggested engineering applications that had been demonstrated in literature. Metamaterials have been adopted in various engineering fields in wide scope, leading to many existing findings, and are still being explored. It is believed

Parameter(s)	Artificial magnetic materials (MNG media)	Artificial electric materials (ENG media)
Commonly adopted unit inclusion	SRR	CSRR
Geometry	See Figure 5(a)	See Figure 5(b)
Equivalent circuit topology	See Figure 6(a)	See Figure 6(b)
Typical response to external electromagnetic field	See Figure 7(a)	See Figure 7(b)

Table 1. Commonly adopted MNG and ENG metamaterial building blocks and their equivalent circuit topologies.

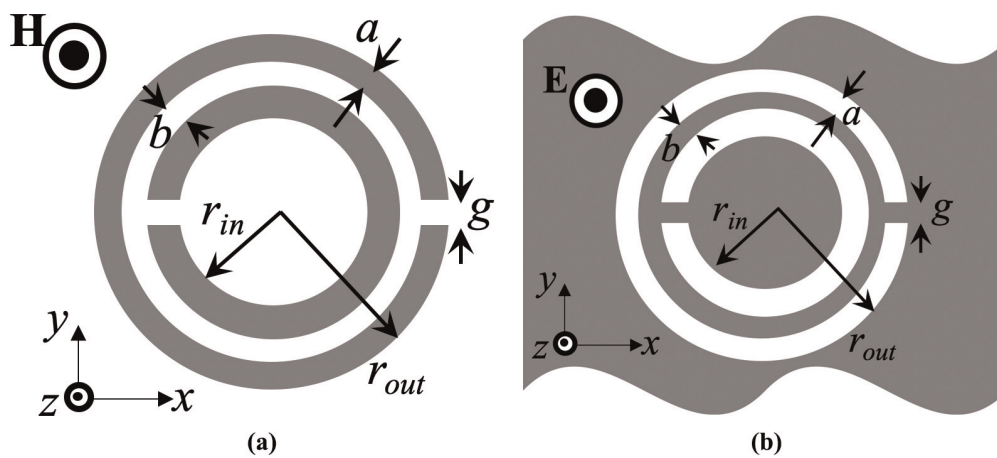


Figure 5. (a) SRR geometry and (b) CSRR geometry.

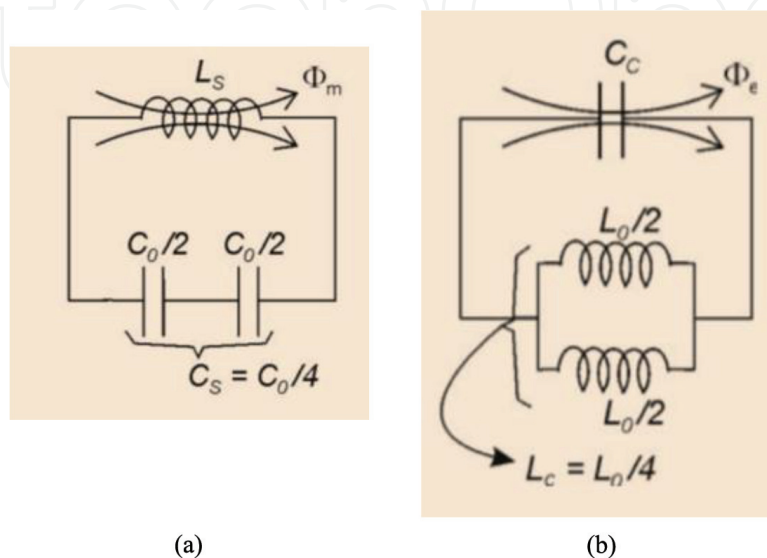


Figure 6. (a) SRR simplified equivalent circuit model and (b) CSRR simplified equivalent circuit model.

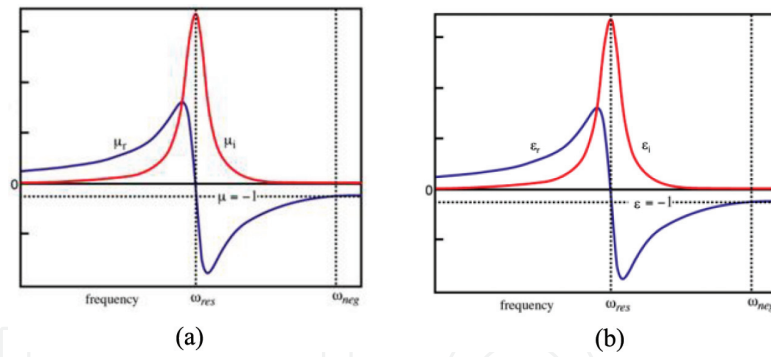


Figure 7. (a) Expected effective permeability response of SRR and (b) expected effective permittivity response of CSRR.

Artificial synthesized metamaterial type	Sign of Re (ϵ)	Sign of Re (μ)	Sign of Im (ϵ)	Sign of Im (μ)	Possible engineering applications
MNG medium	+	-	+	+	<ul style="list-style-type: none"> • Bandstop/band-pass filters for radio frequency/microwave circuits and systems [24, 25] • Mutual coupling reduction between antennas [26–28] • Electromagnetic shielding of electronic circuits and devices [29] • Gain enhancement of antennas, when used as superstrate [30] • Electromagnetic energy harvesting and absorbers [31, 32]
ENG medium	-	+	+	+	<ul style="list-style-type: none"> • Planar, miniaturized filters for radio frequency/microwave and millimeter wave circuits and systems [16–18] • Mutual coupling reduction between antennas [33] • Electromagnetic shielding of electronic circuits and devices [29, 34, 35]
DNG medium	-	-	+	+	<ul style="list-style-type: none"> • Demonstration of backward wave propagation and negative refraction [21, 22, 36] • Focusing, imaging, and superlensing [23, 37] • Invisibility cloaks [38–40]

Table 2. List of general metamaterials families, based on the sign of their constitutive parameters, including possible engineering applications.

that metamaterials can find lots of applications in other physics and engineering areas, especially in the millimeter and terahertz regimes that might not yet have been reported to date. Note that the number of applications is not limited to those listed in **Table 2**.

3. Electromagnetic wave interaction with metamaterials

In this section, the behavior of electromagnetic wave interaction with metamaterials is studied both analytically and numerically. Analytical formulation of electromagnetic field behavior on a one-dimensional artificial lossless and isotropic

metamaterial slab due to an external plane wave excitation is presented first. Numerical demonstration of two-dimensional electromagnetic wave interaction with artificial DNG, MNG, and ENG metamaterial slabs is then illustrated and discussed.

3.1 Normal plane wave interaction with metamaterials

We consider the problem of a uniform plane wave that is traveling along the $+z$ -direction in free space and is incidental normally on an infinitely large metamaterial slab of thickness, h . The metamaterial slab is placed between $z = 0$ and $z = h$, as shown in **Figure 8**, and is made infinitely large along x and y directions. For convenience, the incident electric field of the uniform plane wave will be assumed to be in the $+x$ -direction, while its associated magnetic field will be in $+y$ -direction.

Without loss of generality, the phasor notation will be used to express the total electric and magnetic fields in each region of the problem geometry in **Figure 8**. In region 1, the electric and magnetic fields are given as:

$$\mathbf{E}_0 = (E_0^+ e^{-jk_0 z} + E_0^- e^{jk_0 z}) \mathbf{a}_x \quad (17)$$

$$\mathbf{H}_0 = (H_0^+ e^{-jk_0 z} + H_0^- e^{jk_0 z}) \mathbf{a}_y \quad (18)$$

where E_0^+ , E_0^- , $H_0^+ = E_0^+/\eta_0$, and $H_0^- = -E_0^-/\eta_0$ are the electric and magnetic field amplitudes in the forward and backward directions in region 1 (free space), respectively. The parameters $k_0 = \omega\sqrt{\mu_0\epsilon_0}$, and $\eta_0 = \sqrt{\mu_0/\epsilon_0}$ are the wavenumber and wave impedance in free space, respectively.

In the second region, in which the metamaterial slab is located, the phasor form of total electric and magnetic fields is given as

$$\mathbf{E}_1 = (E_1^+ e^{-jk_1 z} + E_1^- e^{jk_1 z}) \mathbf{a}_x \quad (19)$$

$$\mathbf{H}_1 = (H_1^+ e^{-jk_1 z} + H_1^- e^{jk_1 z}) \mathbf{a}_y \quad (20)$$

where E_1^+ , E_1^- , $H_1^+ = E_1^+/\eta_1$, and $H_1^- = -E_1^-/\eta_1$ are the electric and magnetic field amplitudes in the forward and backward directions in region 2 (metamaterial slab),

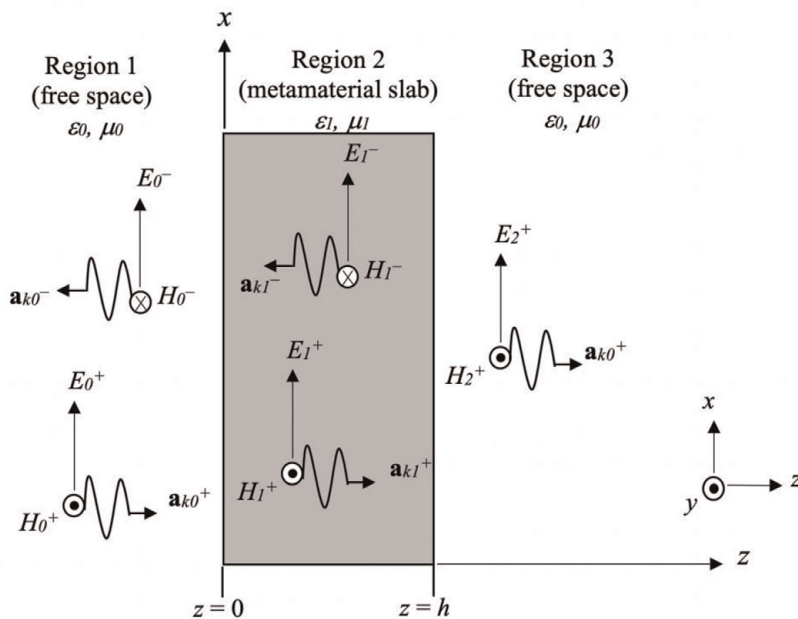


Figure 8.

Normal incidence of a uniform plane wave on an infinitely large metamaterial slab of thickness, h .

respectively. The parameters $k_1 = \omega\sqrt{\mu_1\epsilon_1}$ and $\eta_1 = \sqrt{\mu_1/\epsilon_1}$ are the wavenumber and wave impedance in the metamaterial slab, respectively.

The electric and magnetic fields in region 3, which represents free space, are

$$\mathbf{E}_3 = E_3^+ e^{-jk_0 z} \mathbf{a}_x \quad (21)$$

$$\mathbf{H}_3 = H_3^+ e^{-jk_0 z} \mathbf{a}_y \quad (22)$$

where E_3^+ and $H_3^+ = E_3^+/\eta_0$ are the electric and magnetic field amplitudes in the forward and backward directions in region 3 (free space), respectively.

After applying the boundary conditions at the metamaterial slab walls, $z = 0$ and $z = h$, the following four relations summarizing the relationship between the reflected/transmitted electric field components, E_0^- , E_1^+ , E_1^- , and E_2^+ , respectively, and the incident electric field amplitude, E_0^+ , are obtained:

$$E_0^- = \frac{j(\eta_1^2 - \eta_0^2) \sin(k_1 h)}{2\eta_0\eta_1 \cos(k_1 h) + j(\eta_1^2 + \eta_0^2) \sin(k_1 h)} E_0^+ \quad (23)$$

$$E_1^+ = \frac{\eta_1(\eta_1 + \eta_0) e^{-jk_1 h}}{2\eta_0\eta_1 \cos(k_1 h) + j(\eta_1^2 + \eta_0^2) \sin(k_1 h)} E_0^+ \quad (24)$$

$$E_1^- = \frac{\eta_1(\eta_0 - \eta_1) e^{jk_1 h}}{2\eta_0\eta_1 \cos(k_1 h) + j(\eta_1^2 + \eta_0^2) \sin(k_1 h)} E_0^+ \quad (25)$$

$$E_2^+ = \frac{2\eta_0\eta_1 e^{-jk_0 h}}{2\eta_0\eta_1 \cos(k_1 h) + j(\eta_1^2 + \eta_0^2) \sin(k_1 h)} E_0^+ \quad (26)$$

To simplify Eqs. (23)–(26) further, we define a normalized wave impedance in the metamaterial slab, as $\eta_m = \eta_1/\eta_0 = \sqrt{\mu_r/\epsilon_r}$ and Eqs. (23)–(26) are read as

$$E_0^- = \frac{j(\eta_m^2 - 1) \sin(k_1 h)}{2\eta_0\eta_1 \cos(k_1 h) + j(\eta_m^2 + 1) \sin(k_1 h)} E_0^+ \quad (27)$$

$$E_1^+ = \frac{(\eta_m^2 + \eta_m) e^{-jk_1 h}}{2\eta_m \cos(k_1 h) + j(\eta_m^2 + 1) \sin(k_1 h)} E_0^+ \quad (28)$$

$$E_1^- = \frac{(\eta_m - \eta_m^2) e^{jk_1 h}}{2\eta_m \cos(k_1 h) + j(\eta_m^2 + 1) \sin(k_1 h)} E_0^+ \quad (29)$$

$$E_2^+ = \frac{2\eta_m e^{-jk_0 h}}{2\eta_m \cos(k_1 h) + j(\eta_m^2 + 1) \sin(k_1 h)} E_0^+ \quad (30)$$

where η_m denotes the normalized wave impedance in the metamaterial slab.

Eqs. (28)–(29) can be used to compute the fractional electric field components in the forward and backward directions, i.e., along the three media. In this analytical study, the electric field strength inside an artificial lossless metamaterial slab is computed using Eq. (19), at a frequency of 10 GHz. We consider the case of a very thin subwavelength homogeneous DNG metamaterial slab, where real parts of permittivity and permeability are both negative at 10 GHz. One possible implementation of such artificial DNG medium can be realized with sufficient number of repeated patterns of composite AMM (SRRs) along with periodic arrangement of metallic rods or planar metallic strips, as demonstrated in [21, 22]. Since evanescent (non-propagating) waves are expected to exist inside single-negative media with exponentially decaying electric field, such cases are not considered here.

Figure 9 shows the analytically computed electric field strength as a function of the DNG metamaterial slab of thickness, h . In this study, the overall DNG slab thickness is considered as $h = 10$ mm. The effect of increasing the effective magnetic permeability of the DNG slab from -1 to -10 is also presented, as shown in **Figure 9**, where higher mismatch along the interface of DPS-DNG is observed as the effective permeability is increased. The case of matched DNG constitutive parameters with those of DPS (air medium) shows zero reflection from such an interface, as expected. For convenience, the 2D structure is illuminated with an x -polarized normal incident plane wave that originates from $z = 0$ plane. The plane wave has an electric field amplitude peak of 1.5 kV/m and phase of 0° .

For validation purposes, this problem of interest was numerically modeled and simulated using ANSYS HFSS simulator [41]. **Figure 10** presents the developed structure to study the problem of normal plane wave incidence on a one-dimensional DNG metamaterial slab. One possible excitation of such plane wave can be numerically realized using a set of periodic boundary conditions; in other words, using perfect electric conductor (PEC) and perfect magnetic conductor (PMC) symmetry planes along four sides of the geometry, x -axis and y -axis walls, respectively, ensure plane wave excitation along with proper excitation of the DNG metamaterial slab (see **Figure 10**). Good agreement can be seen between analytically and numerically computed electric field strength inside the DNG metamaterial slab, as shown in **Figures 9** and **11**.

3.2 Numerical demonstration of electromagnetic wave interaction with artificial DNG, MNG, and ENG metamaterial slabs

In this section, numerical demonstration of electromagnetic cylindrical wave interaction with various artificial isotropic and lossy metamaterial slabs is illustrated. **Figure 12** depicts the numerical full-wave simulation model, where an artificial lossy DNG slab was placed between two natural, lossy DPS slabs. In this numerical study, DPS, DNG, and MNG media are all considered as lossy and isotropic, where for the case of DNG slab, effective constitutive parameters are $\epsilon_r = -1$ and $\mu_r = -2.2$, with dielectric and magnetic losses of 0.002 , while the constitutive parameters are $\epsilon_r = 2.2$ and $\mu_r = -1$ for the MNG medium case, and $\epsilon_r = -2.2$ and $\mu_r = 1$ for the ENG medium slab case, with similar losses as those

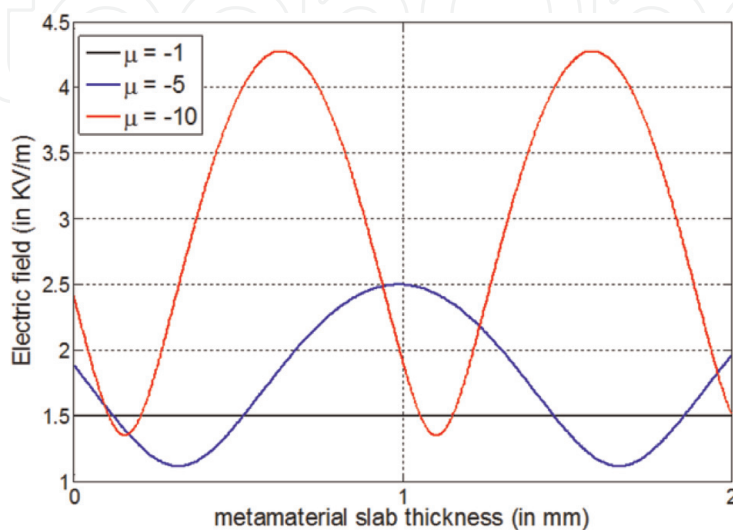


Figure 9. Analytical computation of electric field strength inside a lossless DNG metamaterial slab. Note that in this study, ϵ_r was set as -1 .

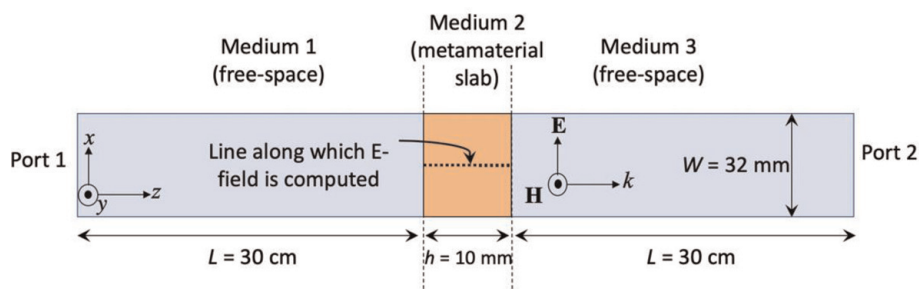


Figure 10.
 The numerical full-wave model used to study the normal incidence of plane wave on a one-dimensional DNG lossless metamaterial slab.

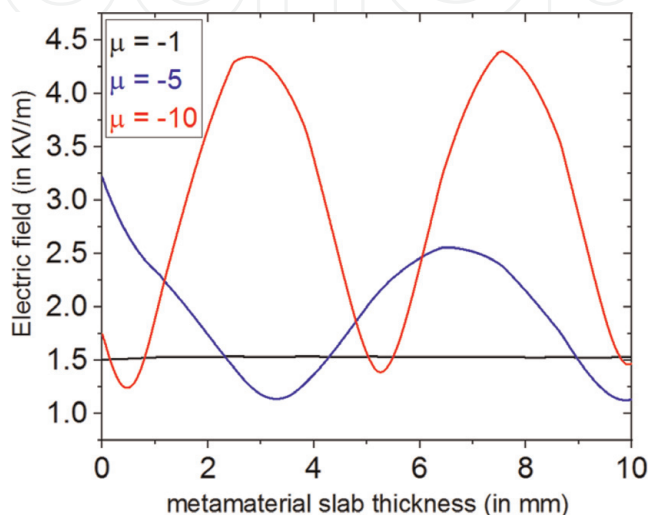


Figure 11.
 Numerical computation of electric field strength inside a lossless DNG metamaterial slab. Note that in this study, ϵ_r was set as -1.

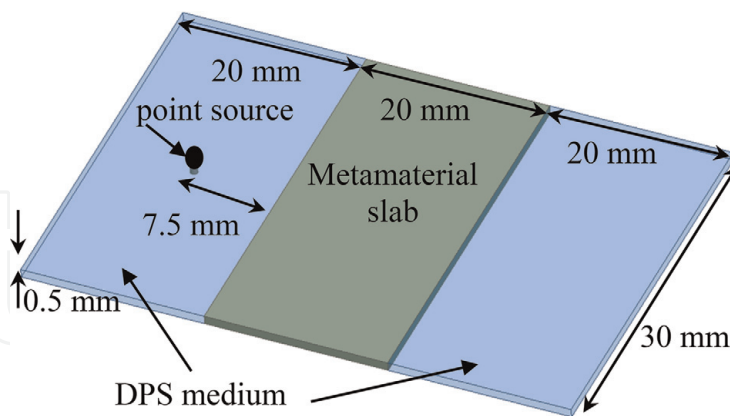


Figure 12.
 Numerical model used to study the electromagnetic wave interaction with DNG medium.

considered in the DNG slab. The constitutive parameters of the DPS medium are $\epsilon_r = 2.2$ and $\mu_r = 1$, with dielectric and magnetic losses of 0.002. Cylindrical waves were excited from a point source that was placed 7.5 mm away from all the aforementioned slabs. For the electromagnetic wave interaction with MNG medium, the DNG medium in **Figure 12** is replaced with MNG medium. The same is also applied to ENG medium. This numerical demonstration was carried out using the numerical full-wave simulator of ANSYS HFSS.

Figure 13 presents the electric field intensity distribution for the DNG, MNG, and ENG media that were captured at a phase of 0 degree and compared against the

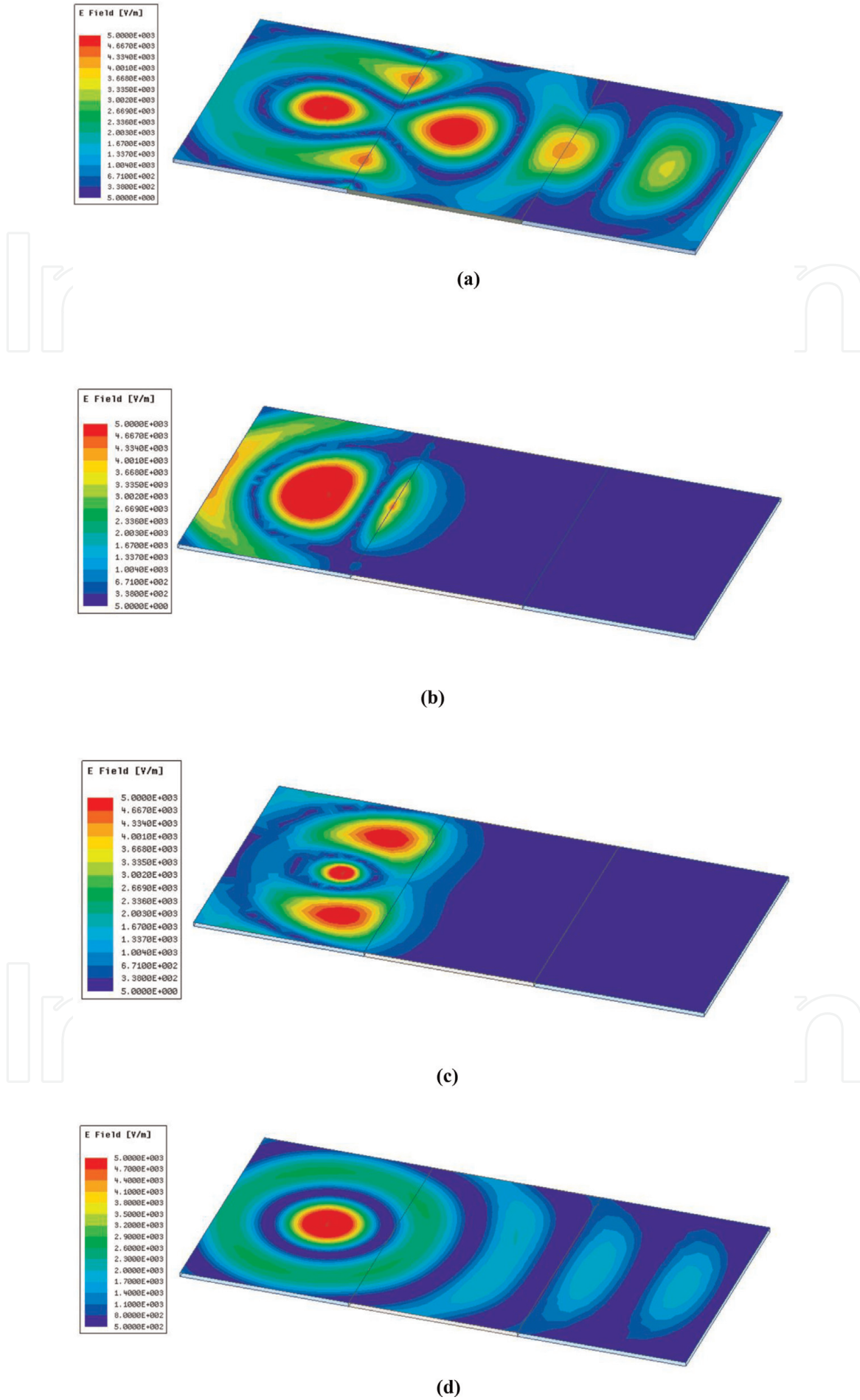


Figure 13. Numerically computed electric field intensity distribution for the studied lossy isotropic homogenized slabs of (a) DNG medium, (b) MNG medium, (c) ENG medium, and (d) reference DPS medium.

reference case of lossy DPS slab. In **Figure 13(a)**, which represents the DNG case, several interesting features can be observed, including negatively refracted waves inside the DNG slab and backward wave propagation (see animated figure, **Figure 14(a)** as compared against the DPS case of **Figure 14(b)**), and focusing phenomena of the original electromagnetic cylindrical waves can be seen at the middle of the DNG slab and also at the DPS slab next to the DNG exit face, in which focusing depends on the selection of the refractive indices along with the DNG medium slab thickness.

While electromagnetic wave propagation inside DNG medium is permissible, since both permittivity and permeability are negative and hence result in a positive real wavenumber, evanescent (non-propagating) waves exist in the MNG medium, as shown in **Figure 13(b)**, that only propagate along the interface and decay exponential away from the MNG slab. This is because in the MNG medium, only the permeability is negative, which results in an imaginary negative wavenumber (see Eq. (7)). Similar behavior to the MNG case is also expected for the single-negative ENG medium slab, as shown in **Figure 13(c)**, where evanescent decaying waves are only present in such single-negative medium. For comparison, the case of all DPS media showed normal forward electromagnetic propagation in such lossy media, as shown in **Figure 13(d)**.

A one-dimensional plot of electric field profile inside the aforementioned artificial metamaterials DNG, MNG, and ENG slabs is also presented as shown in **Figure 15** and compared against the normal dielectric DPS medium case. As can be seen from **Figure 15**, propagating electromagnetic field inside the DNG medium

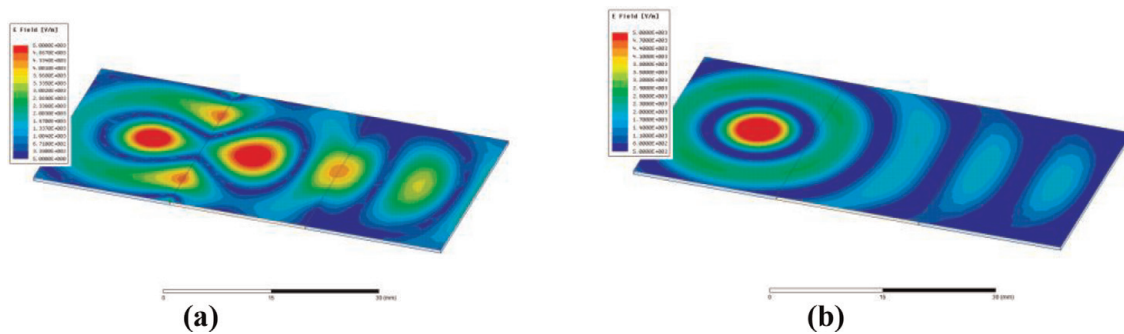


Figure 14. Animated snapshots for the electric field distribution for (a) DNG medium and (b) DPS medium cases.

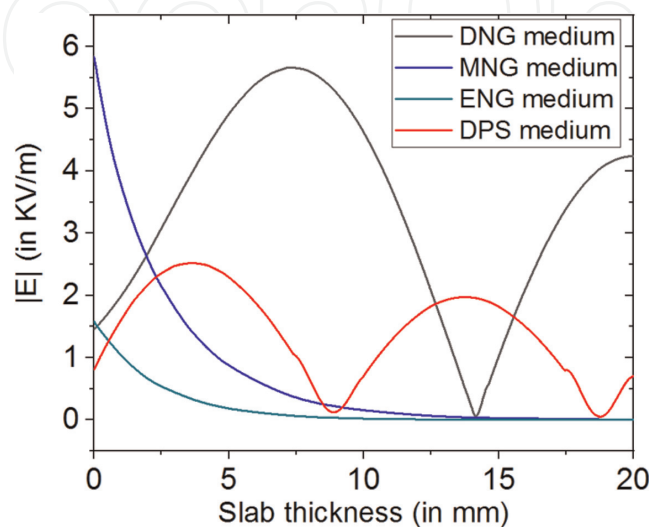


Figure 15. A one-dimensional plot of electric field strength inside the (a) DNG medium, (b) MNG medium, (c) ENG medium, and (d) DPS medium.

slab is visible through the recorded electric field profile at a frequency of 10 GHz. Unlike electric field behavior inside the DNG medium, exponentially decaying electric field profile is recorded inside the single-negative MNG and ENG media slabs. Despite the fact that non-propagating (evanescent) waves existed in both MNG and ENG media slabs, the electric field profile is much stronger at the DPS-MNG interface than the strength at the DPS-ENG interface.

4. Conclusions

In this chapter, a short review of metamaterials and their realizations based on subwavelength resonant inclusions was presented, along with suggested real-world metamaterial engineering applications that were explored and presented in literature. Over the past 20 years, much interest from researchers and industry was seen to target the use of artificial DNG metamaterials for various engineering applications and physics-based problems. It is important to highlight here that although single-negative media do not permit electromagnetic wave propagation, such artificial media are good candidates for various electromagnetic waves filtering scenarios and harmonic suppression, since they provide high level of electromagnetic wave mitigation and ease of fabrication and integration with radio frequency/microwave circuits and systems.

Analytical and numerical studies of electromagnetic field behavior and response inside an artificial metamaterial medium were presented. Firstly, the problem of a one-dimensional normal plane wave incidence on an artificial DNG metamaterial slab was analytically formulated, and results were discussed. Furthermore, numerical demonstrations of two-dimensional electromagnetic wave interaction with various lossy metamaterial slabs DNG, MNG, and ENG media were presented and discussed.

Conflict of interest


The author declares that there is no conflict of interest in the publication of this book chapter.

Author details

Mohammed M. Bait-Suwailam
Sultan Qaboos University, Muscat, Oman

*Address all correspondence to: msuwailem@squ.edu.om

IntechOpen

© 2019 The Author(s). Licensee IntechOpen. This chapter is distributed under the terms of the Creative Commons Attribution License (<http://creativecommons.org/licenses/by/3.0>), which permits unrestricted use, distribution, and reproduction in any medium, provided the original work is properly cited. 

References

- [1] Jackson JD. *Classical Electrodynamics*. New York: Wiley; 1998
- [2] Pendry JB, Holden AJ, Stewart WJ, Youngs I. Extremely low frequency plasmons in metallic mesostructures. *Physical Review Letters*. 1996;**76**: 4773-4776
- [3] Pendry JB, Holden AJ, Robbins DJ, Stewart WJ. Magnetism from conductors and enhanced nonlinear phenomena. *IEEE Transactions on Microwave Theory and Techniques*. 1999;**47**:2075-2084
- [4] Veselago VG. The electrodynamics of substances with simultaneously negative values of ϵ and μ . *Soviet Physics Uspekhi*. 1968;**10**:509-514
- [5] Smith DR, Vier DC, Kroll N, Schultz S. Direct calculation of permeability and permittivity for a left-handed metamaterial. *Applied Physics Letters*. 2000;**77**:2246-2248
- [6] Smith DR, Vier DC, Koschny T, Soukoulis CM. Electromagnetic parameter retrieval from inhomogeneous metamaterials. *Physical Review E*. 2005;**71**: 036617-036628
- [7] Simovski CR, Tretyakov SA. Local constitutive parameters of metamaterials from an effective-medium perspective. *Physical Review B*. 2007;**75**:195111
- [8] Maslovski S, Ikonen P, Kolmakov I, Tretyakov S, Kaunisto M. Artificial magnetic materials based on the new magnetic particle: Metasolenoid. *Progress in Electromagnetics Research*. 2005;**54**:61-81
- [9] Callister WD. *Materials Science and Engineering, An Introduction*. John Wiley and Sons Inc; 2000
- [10] Schelkunoff SA, Friis HT. *Antennas: Theory and Practice*. New York: Wiley; 1952
- [11] Marqués R, Medina F, Rafii-El-Idrissi R. Role of bianisotropy in negative permeability and left-handed metamaterials. *Physical Review B*. 2002;**65**:144440(1)-144440(6)
- [12] Marqués R, Mesa F, Martel J, Medina F. Comparative analysis of edge- and broadside-coupled split ring resonators for metamaterial design-theory and experiments. *IEEE Transactions on Antennas and Propagation*. 2003;**51**:2572-2581
- [13] Baena JD, Marqués R, Medina F, Martel J. Artificial magnetic metamaterial design by using spiral resonators. *Physical Review B: Condensed Matter and Materials Physics*. 2004;**69**:014402(1)-014402(5)
- [14] Yousefi L, Ramahi OM. Artificial magnetic materials using fractal Hilbert curves. *IEEE Transactions on Antennas and Propagation*. 2010;**58**: 2614-2622
- [15] Pines D, Bohm D. A collective description of electron interactions: II. Collective vs individual particle aspects of the interactions. *Physical Review*. 1952;**85**:338
- [16] Falcone F, Lopetegi T, Baena JD, Marqués R, Martín F, Sorolla M. Effective negative- ϵ stopband microstrip lines based on complementary split ring resonators. *IEEE Microwave and Wireless Components Letters*. 2004;**14**:280-282
- [17] Falcone F, Lopetegi T, Laso MAG, Baena JD, Bonache J, Beruete M, et al. Babinet principle applied to the design of metasurfaces and metamaterials. *Physical Review Letters*. 2004;**93**: 197401(1)-197401(4)

- [18] Baena J, Bonache J, Martín F, Marqués R, Falcone F, Lopetegi T, et al. Equivalent-circuit models for split-ring resonators and complementary split-ring resonators coupled to planar transmission lines. *IEEE Transactions on Microwave Theory and Techniques*. 2005;**53**:1451-1461
- [19] Booker HG. Slot aeriels and their relation to complementary wire aeriels (Babinet's principle). *Journal of the Institute of Electrical Engineers*. 1946;**93**(pt. III-A):620-626
- [20] Bait-Suwailam MM, Yousefi L, Alavikia B, Ramahi OM. Analytical models for predicting the effective permittivity of complementary metamaterial structures. *Microwave and Optical Technology Letters*. 2013;**55**:1565-1569
- [21] Smith DR, Padilla WJ, Vier DC, Nemat-Nasser SC, Schultz S. Composite medium with simultaneously negative permeability and permittivity. *Physical Review Letters*. 2000;**84**:4184-4187
- [22] Shelby RA, Smith DR, Schultz S. Experimental verification of a negative index of refraction. *Science*. 2001;**292**:77-79
- [23] Pendry JB. Negative refraction makes a perfect lens. *Physical Review Letters*. 2000;**85**:3966-3969
- [24] Marqués R, Martín F, Sorolla M. *Metamaterials With Negative Parameters: Theory, Design and Microwave Applications*. Hoboken, NJ: Wiley; 2008
- [25] Gil M, Bonache J, Gil I, García-García J, Martín F. Miniaturization of planar microwave circuits by using resonant-type left handed transmission lines. *IET Microwave Antennas and Propagation*. 2007;**1**:73-79
- [26] Ferrer PJ, Gonzalez-Arbesu JM, Romeu J. Decorrelation of two closely spaced antennas with a metamaterial AMC surface. *Microwave and Optical Technology Letters*. 2008;**50**:1414-1417
- [27] Rajo-Iglesias E, Quevedo-Teruel O, Inclan-Sanchez L. Planar soft surfaces and their application to mutual coupling reduction. *IEEE Transactions on Antennas and Propagation*. 2009;**57**:3852-3859
- [28] Bait-Suwailam MM, Boybay MS, Ramahi OM. Electromagnetic coupling reduction in high-profile monopole antennas using single-negative magnetic metamaterials for MIMO applications. *IEEE Transactions on Antennas and Propagation*. 2010;**58**:2894-2902
- [29] Celozzi S, Araneo R, Lovat G. *Electromagnetic Shielding*. Wiley-IEEE Press; 2008. ISBN: 978-0-470-05536-6
- [30] Attia H, Yousefi L, Bait-Suwailam MM, Boybay MS, Ramahi OM. Enhanced-gain microstrip antenna using engineered magnetic superstrates. *IEEE Antennas and Wireless Propagation Letters*. 2009;**8**:1198-1201
- [31] Ramahi OM, Almoneef TS, AlShareef M, Boybay MS. Metamaterial particles for electromagnetic energy harvesting. *Applied Physics Letters*. 2012;**101**:173903
- [32] Watts CM, Liu X, Padilla WJ. Metamaterial electromagnetic wave absorbers. *Advanced materials*. 2012;**24**:98-120
- [33] Bait-Suwailam MM, Siddiqui OF, Ramahi OM. Mutual coupling reduction between microstrip patch antennas using slotted-complementary split-ring resonators. *IEEE Antennas and Wireless Propagation Letters*. 2010;**9**:876-878
- [34] Casey KF. Electromagnetic shielding behavior of wire-mesh screens. *IEEE Transactions on Electromagnetic Compatibility*. 1988;**30**:298-306

[35] Bait-Suwailam MM, Ramahi OM. Ultrawideband mitigation of simultaneous switching noise and EMI reduction in high-speed PCBs using complementary split-ring resonators. *IEEE Transactions on Electromagnetic Compatibility*. 2012;**54**:389-396

[36] Eleftheriades GV, Iyer AK, Kremer PC. Planar negative refractive index media using periodically LC loaded transmission lines. *IEEE Transactions on Microwave Theory and Techniques*. 2002;**50**:2702-2712

[37] Eleftheriades GV, Siddiqui OF. Negative refraction and focusing in hyperbolic transmission-line periodic grids. *IEEE Transactions on Microwave Theory and Techniques*. 2005;**53**: 396-403

[38] Schurig D, Mock J, Justice BJ, Cummer SA, Pendry JB, Starr AF, et al. Metamaterial electromagnetic cloak at microwave frequencies. *Science*. 2006; **314**:977-980

[39] Ergin T, Stenger N, Brenner P, Pendry JB, Wegener M. Three-dimensional invisibility cloak at optical wavelengths. *Science*. 2010;**328**:337-339

[40] Selvanayagam M, Eleftheriades GV. An active electromagnetic cloak using the equivalence principle. *IEEE Antennas and Wireless Propagation Letters*. 2012;**11**:1226-1229

[41] ANSYS® Electromagnetics Suite, 17.2 [Online], <http://www.ansys.com> 熱